Research report D3.1

Characterization of 316L weld samples

Eklavya Koshta, Risto Ilola

Table of Contents

1 Introduction

This report presents results of WP3 Thermally Induced Stress Corrosion Cracking in the TOFFEE project Total Fatigue Life in Plant Environment at Aalto University. The research consists of sample characterization after autoclave exposure tests and investigation of properties of the 316L weld in as-welded condition.

Stress corrosion cracking (SCC) is a complex phenomenon that occurs when a susceptible material is exposed to a corrosive environment under tensile stress. In nuclear systems, the primary contributors to SCC are residual stresses introduced during welding, thermal cycles during operation, and the high-temperature water environment. Studies have shown that tensile residual stresses can significantly accelerate crack initiation and growth under the service conditions [1]. Cold work, thermal aging, and sensitization further increase the susceptibility to SCC.

Thermal gradients caused by fluctuating operating conditions can lead to uneven plastic deformation, resulting in residual stress buildup. These stresses may remain hidden but become critical when combined with environmental exposure and mechanical loading [2]. Research has also indicated that even without external loading, the combination of thermal stresses and microstructural changes can lead to SCC initiation in localized regions.

Austenitic stainless steels, particularly grade 316L, are widely used in nuclear power plants due to their excellent corrosion resistance, mechanical strength, and weldability. However, these materials remain susceptible to SCC. Previous studies have demonstrated that welding-induced tensile residual stresses, together with high-temperature water and thermal fluctuations, can significantly increase the likelihood of SCC initiation and propagation [3].

Building upon earlier research conducted under the TOFFEE 2024 project, this study continues the investigation of microstructure and properties of welded 316L pipe samples in as-welded condition and after autoclave exposure tests. Earlier study indicated that residual stresses generated in welding and subsequent thermal cycling did not result in crack formation during autoclave exposure tests in simulated PWR conditions despite the high stress levels of order of 500 MPa in the tested samples [4].

The report contains the following results:

- Measurements of residual stresses in as-welded condition and after autoclave exposure tests for thermally cycled weld samples using X-ray diffraction (XRD) technique.
- Characterization of pipe weld microstructure in as-welded condition using SEM EBSD (scanning electron microscope electron backscatter diffraction) and LOM (light optical microscopy).
- Measurements of microhardness profiles of selected samples.

2 Experimental methods

2.1 Materials

The test material investigated this study was 316L austenitic stainless steel. Two rings of 150 mm in length of austenitic 316L stainless steel pipe (diameter 326 mm, thickness 33 mm, Figure 1) were received from VTT. The material represents the material used in OL3 primary cooling circuit. Chemical composition of the pipe material is presented in Table 1. The 150 mm long pipe rings were welded together at Suisto Engineering with NG-GTAW method using 316LSi filler metal (Table 1). The welding was done according to a WPS received from TVO, so that the weld represents the OL3 primary circuits welds.

Table 1. Chemical composition of the pipe material and filler metal.

	C	Mn	Si	P	S	Cr	Ni	Mo	Cu	N
Base material	0.028	1.81	0.39	0.022	0.002	17.1	12.03	2.27	0.56	0.08
Filler metal	0.02	1.8	0.85	0.023	0.002	18.3	11.4	2.5	0.2	0.073

Three segments of 140 mm x 65 mm in size were cut from the welded pipe for SCC tests in autoclaves at VTT. Prior to the autoclave exposure test, selected positions of the weld root were thermally cycled in order to introduce high residual stress levels into them. Average grain size (G) of the base material is 6 (44 µm). Microstructures of the base material and weld are presented in [4] and [5].

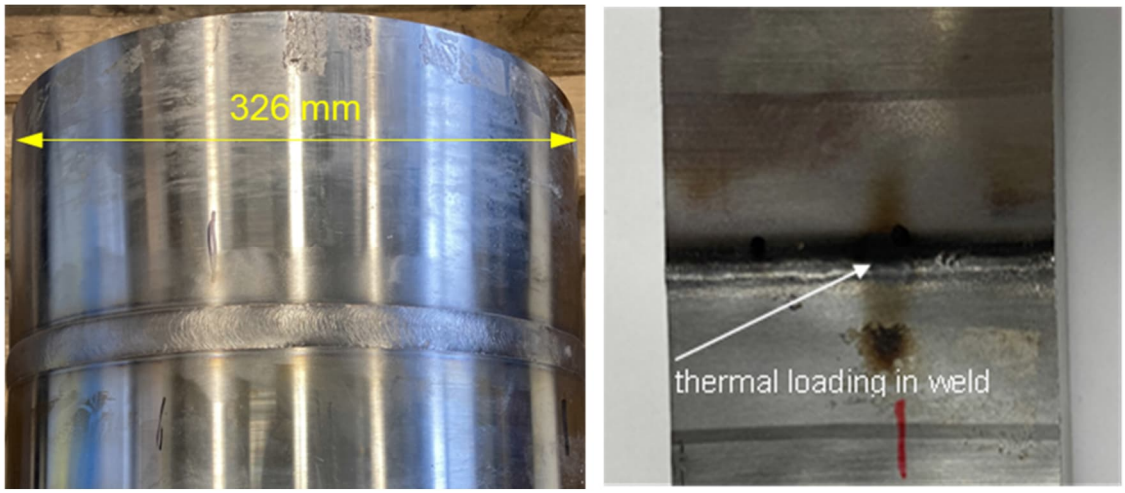

Figure 1. 316L pipe welded with NG-GTAW method (left) and location of thermal cycling on the inner surface of the pipe (right).

2.2 Residual stress measurements

Residual stresses were measured from the weld root and HAZ in as-welded condition and after autoclave tests XRD measurements to characterize the residual stress distribution. The measurements were conducted using a Stresstech XStress 3000 G2R diffractometer, as presented in Figure 2.

Figure 2. Residual stress measurement setup.

Principal stresses ($\sigma_{1,2}$) and their direction (θ) were calculated using Equations 1-3 with following stresses.

- σ_x: residual stress in the axial direction (0°),
- σ_y: residual stress in the hoop direction (90°), and
- $\sigma_{45°}$: stress at a 45° diagonal direction.

In the stress analysis, the stress state was considered as two-dimensional (plane stress), where the through-thickness stress component is negligible ($\sigma_z \approx 0$). The three key in-plane normal stresses measured through the equipment are:

$$\sigma_{1,\ 2} = \frac{\sigma_x + \sigma_y}{2} \pm \sqrt{\left(\frac{\sigma_x - \sigma_y}{2}\right)^2 + {\sigma_{xy}}^2} \quad (1)$$

$$\sigma_{xy} = \sigma_{45^o} - \frac{\sigma_x + \sigma_y}{2} \quad (2)$$

$$tan\ 2\theta = \frac{2\sigma_{xy}}{\sigma_x - \sigma_y} \quad (3)$$

2.3 SEM EBSD analysis

SEM EBSD was used to study the grain structure, orientation, and grain boundary character in the weld and HAZ regions. The analysis was performed using a JEOL JIB-4700F SEM instrument. The system enables simultaneous SEM imaging and crystallographic mapping through backscattered electron diffraction. Figure 3 shows the SEM + EBSD system (JEOL JIB-4700F – NMC) used to acquire high-resolution EBSD maps of the sample.

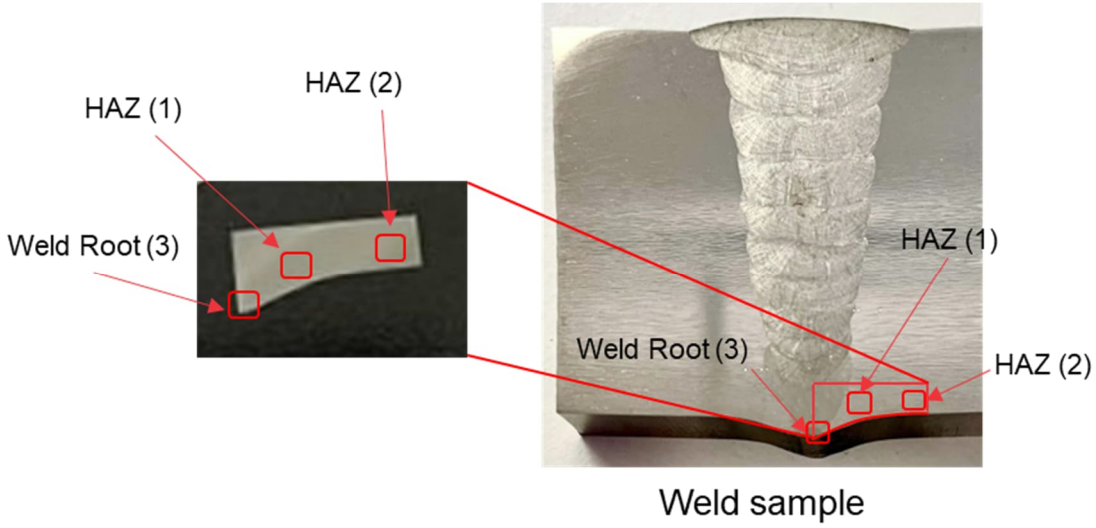

Figure 3. Locations of EBSD analyses in as-welded 316L pipe sample.

2.3.1 Microhardness testing

Microhardness testing was performed across the weld cross-section to study hardness variation in the weld and HAZ regions. The measurements were done using a Struers Duramin-40 AC2 hardness tester from as-welded and autoclave tested (thermally cycled at 500° C) specimens. Measurement load used was 0.02 kg.

2.3.2 Optical microscopy

Weld and base material microstructures were examined using Zeiss Axio optical microscope. The samples were plane ground and polished mechanically and etched electrochemically in a 60% HNO_3 + 40 % H_2O solution using 3 V current.

2.3.3 Ferrite measurement

Ferrite content was measured using Feritscope® MP3C instrument from the as-welded sample from different locations of weld and base metal.

3 Results and discussion

3.1 XRD residual stress analysis

3.1.1 As-welded condition

The as-welded segment of the pipe weld used in residual stress measurements and the location of the measurements are presented in Figure 4. The measurements showed compressive residual stresses at the weld centerline (Figure 5). The stresses increased gradually when moving towards the base metal and changed to tensile stresses. The maximum tensile residual stresses about 200 MPa occurred in the base material at the border of the visible HAZ about 10 mm distance from the weld centerline (Figure 5). After that, the stresses reversed to compressive on both sides of the weld root. The results are presented in Table 2.

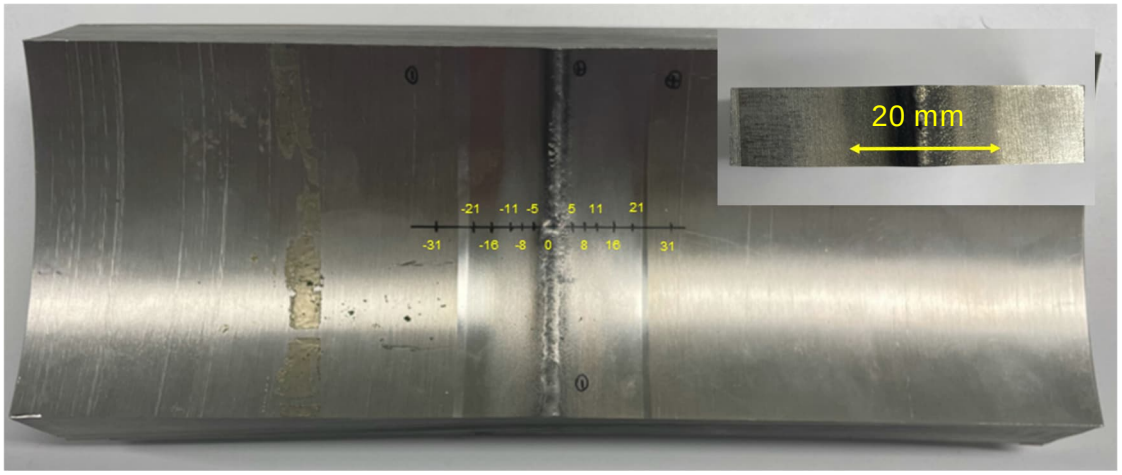

Figure 4. Segment of as-welded pipe used in residual stress measurements and size of the visible HAZ on the root side.

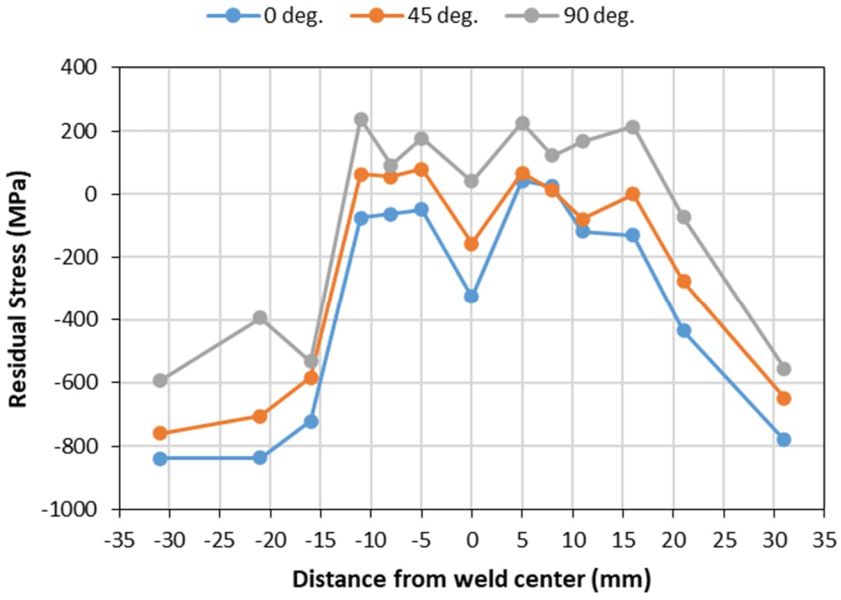

Figure 5. Residual stresses in the as-welded sample.

Table 2. Measured residual stresses and calculated principal stresses in as-welded sample.

Along x-axis, mm	Residual stress, MPa (at 0°)	Residual stress, MPa (at 45°)	Residual stress, MPa (at 90°)	Shear stress (σ_{xy}), MPa	Principal stress (σ_1), MPa	Principal stress (σ_2), MPa	Principal angle θ °
-31	-840	-760	-593	-44	-585	-847	10
-21	-837	-706	-394	-91	-376	-855	11
-16	-722	-583	-533	44	-523	-732	-12
-11	-76	63	238	-18	239	-77	3
-8	-64	55	92	41	102	-74	-14
-5	-49	79	177	15	178	-50	-4
0	-325	-157	41	-15	42	-326	2
5	42	67	225	-66	246	20	18
8	25	13	121	-60	150	-4	26
11	-119	-79	167	-104	200	-152	18
16	-131	0	213	-42	218	-136	7
21	-436	-277	-73	-23	-71	-437	4
31	-781	-648	-556	21	-554	-783	-5

3.1.2 Thermally cycled samples before autoclave exposure tests

Before the autoclave exposure tests, the samples underwent thermal cycling in which peak temperatures were 300, 400, and 500°C, respectively. Thermal cycling increased markedly the tensile residual stresses in the welded to a level of about 500 MPa, but in the samples thermally cycled at 300 and 400°C, the residual maximum tensile residual stresses were close to values in the as-welded condition. The data is presented in [4] and the principal stresses calculated from that are presented in Tables 3-5.

Table 3. Principal stresses calculated from sample thermally cycled at 300 °C before autoclave exposure test.

Along x-axis, mm	Residual stress, MPa (at 0°)	Residual stress, MPa (at 45°)	Residual stress, MPa (at 90°)	Shear stress (σ_{xy}), MPa	Principal stress (σ_1), MPa	Principal stress (σ_2), MPa	Principal angle θ °
5	108	78	86	-19	119	75	-30
10	-146	8	152	6	152	-147	-1
30	-669	-472	-189	-43	-185	-673	5

Table 4. Principal stresses calculated from sample thermally cycled at 400 °C before autoclave exposure test.

Along x-axis, mm	Residual stress, MPa (at 0°)	Residual stress, MPa (at 45°)	Residual stress, MPa (at 90°)	Shear stress (σ_{xy}), MPa	Principal stress (σ_1), MPa	Principal stress (σ_2)	Principal angle θ (°)
5	270	158	113	-34	277	106	-12
10	154	144	153	-10	163	144	-44
30	-710	-469	-223	-3	-223	-710	0

Table 5. Principal stresses calculated from sample thermally cycled at 500 °C before autoclave exposure test.

Along x-axis, mm	Residual stress, MPa (at 0°)	Residual stress, MPa (at 45°)	Residual stress, MPa (at 90°)	Shear stress (σ_{xy}), MPa	Principal stress (σ_1), MPa	Principal stress (σ_2), MPa	Principal angle θ °
5	565	459	311	21	566	309	5
10	658	515	335	18	659	334	3
30	-182	23	206	11	206	-182	-2

Also in these samples, the maximum tensile residual stresses occurred in HAZ at about 10 distance from the weld centerline.

3.1.3 Thermally cycled samples after autoclave exposure tests

Sample thermally cycled at 300 °C

No significant tensile residual stress reduction was observed after the autoclave exposure test (Figure 6). Also, when moving away from the centerline towards the HAZ, the residual stress pattern was similar to that of the as-welded condition. At the weld centerline, the stresses were compressive, then they increased and changed to tensile stresses, and then changed again into compressive stresses after HAZ. Residual stress values and calculated principal stresses are presented in Table 6.

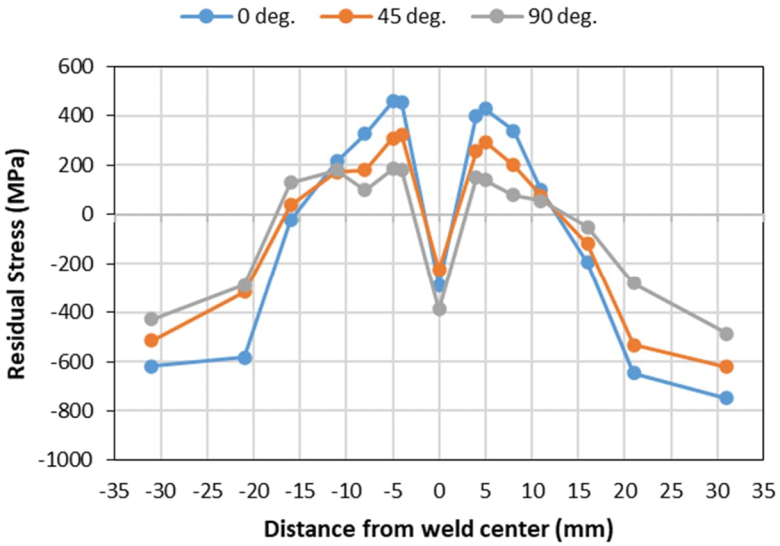

Figure 6. Residual stresses in the sample thermally cycled at 300 °C after autoclave exposure test.

Table 6. Residual stress values and calculated principal stresses in 300 °C thermally cycled sample after autoclave exposure test.

Along x-axis, mm	Residual stress, MPa (at 0°)	Residual stress, MPa (at 45°)	Residual stress, MPa (at 90°)	Shear stress (σ_{xy}), MPa	Principal stress (σ_1), MPa	Principal stress (σ_2), MPa	Principal angle θ °
-31	-619	-516	-428	8	-428	-619	-2
-21	-584	-316	-288	119	-246	-626	-19
-16	-23	39	129	-14	130	-24	5
-11	216	174	181	-25	229	168	-28
-8	327	179	98	-34	332	93	-8
-5	460	310	185	-13	461	184	-3
-4	457	324	182	5	457	182	1
0	-288	-225	-388	113	-214	-462	33
4	402	256	149	-19	403	148	-4
5	428	295	140	12	428	139	2
8	341	200	79	-10	342	79	-2
11	99	77	55	1	99	55	1
16	-196	-119	-50	3	-50	-196	-1
21	-647	-534	-281	-70	-268	-660	10
31	-749	-623	-488	-4	-488	-749	1

Sample thermally cycled at 400 °C

Also, for the sample that was thermally cycled at 400 °C, there was not observed significant residual stress relaxation during the autoclave exposure test (Figure 7 and Table 7). Tensile residual stresses were present in HAZ. Some variation in the stress profile was observed on the different sides of the weld centerline.

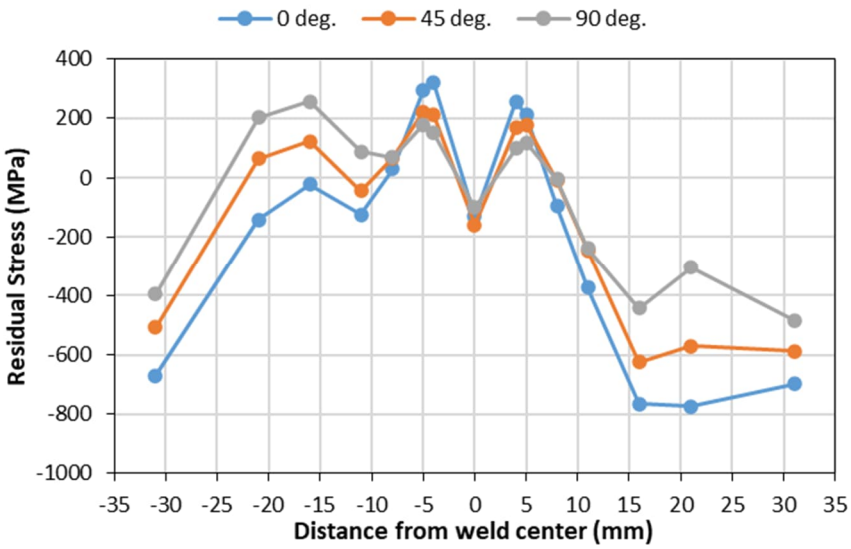

Figure 7. Residual stresses in the sample thermally cycled at 400 °C after autoclave exposure test.

Table 7. Residual stress values and calculated principal stresses in 400 °C thermally cycled sample after autoclave exposure test.

Along x-axis, mm	Residual stress, MPa (at 0°)	Residual stress, MPa (at 45°)	Residual stress, MPa (at 90°)	Shear stress (σ_{xy}), MPa	Principal stress (σ_1), MPa	Principal stress (σ_2), MPa	Principal angle θ °
-31	-671	-508	-396	26	-394	-674	-5
-21	-142	65	202	35	206	-146	-6
-16	-23	123	256	6	257	-23	-1
-11	-125	-44	88	-25	90	-127	7
-8	31	67	68	18	75	23	-22
-5	296	222	178	-15	298	176	-7
-4	319	212	150	-23	322	147	-7
0	-131	-159	-101	-43	-71	-161	35
4	257	168	99	-10	257	99	-4
5	210	178	118	14	212	116	8
8	-96	-10	-5	40	10	-111	-21
11	-374	-245	-240	62	-216	-398	-21
16	-765	-626	-442	-22	-441	-766	4
21	-774	-571	-304	-32	-302	-776	4
31	-698	-589	-483	1	-483	-698	0

Sample thermally cycled at 500 °C

Sample that was thermally cycled at 500 °C had been cut for SEM analysis in earlier investigations [4] and a reliable stress measurement was not possible to be performed. However, tensile residual stresses were present in HAZ

3.2 SEM EBSD analysis and ferrite measurement

The analysis focused on three distinct regions across the weld: HAZ (1), HAZ (2), and fusion zone on the weld root side (Figure 3, page 6). All samples were investigated in as-polished condition after polishing with 0.02 μm colloidal silica.

3.2.1 As-welded sample

Misorientation (MO) average maps

A higher average misorientation was observed at grain boundaries than inside the grains when measured from HAZ close to weld root (point 1, Figure 8). This indicates stress accumulation at grain boundaries during manufacturing and welding processes of the pipe. Further from the weld root in HAZ (point 2, Figure 8) the average misorientation was low, and in the fusion zone between the points 1 and 2 in HAZ. In these regions the stress accumulation is considered as low.

Inverse pole figure (IPF) maps

Inverse pole figure maps from as-welded sample are presented in Figure 9. They showed clearly elongated grains in HAZ point 1 (Figure 9) indication plastic deformation during pipe manufacturing and welding. In HAZ point 2 (Figure 9) the grains were more equiaxed. In the weld fusion zone (point 3, Figure 9), the microstructure was typical to an austenitic steel weld showing a second phase mixed with austenite.

Phase maps

Phase maps showed that second phase in the weld was delta ferrite and its content was about 4 % in the weld (point 3, Figure 10). In the measurements with Feritscope® MP3C instrument, the detected delta ferrite content in the weld was 4-8%, which is in accordance with the EBSD analysis. In HAZ point 1 (Figure 10), the delta ferrite content was below 1 %, which was the same than in the Feritscope® measurements for the base material. Individual delta ferrite stringers were found in the base material in LOM investigations [5].

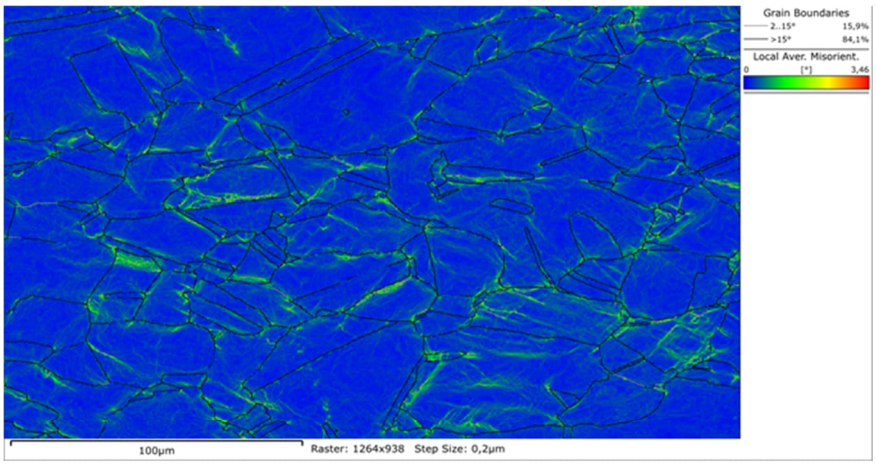

HAZ MO average map (Point 1)

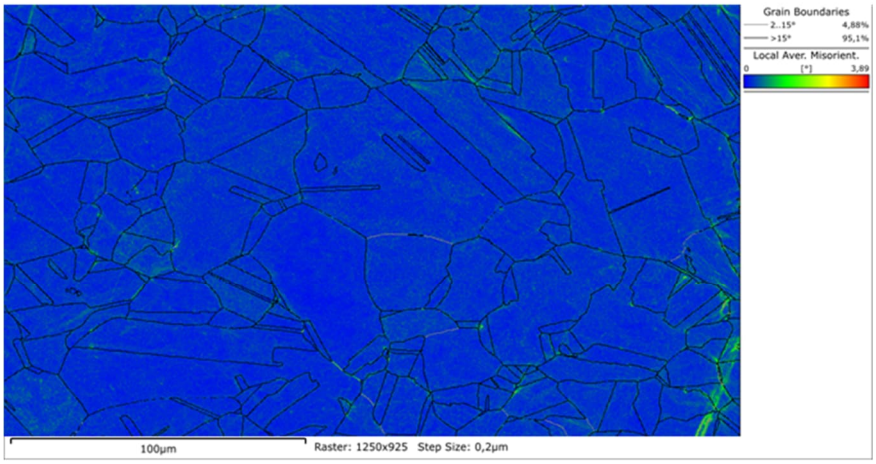

HAZ MO average map (Point 2)

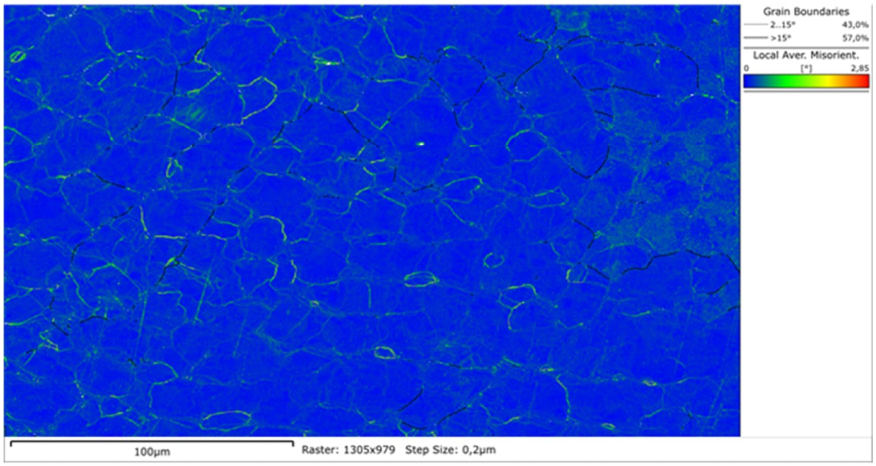

Fusion Zone MO average map (Point 3)

Figure 8. Average misorientation maps showing greater stress accumulation at grain boundaries in HAZ point 1 than in HAZ point 2 and fusion zone in as-welded sample.

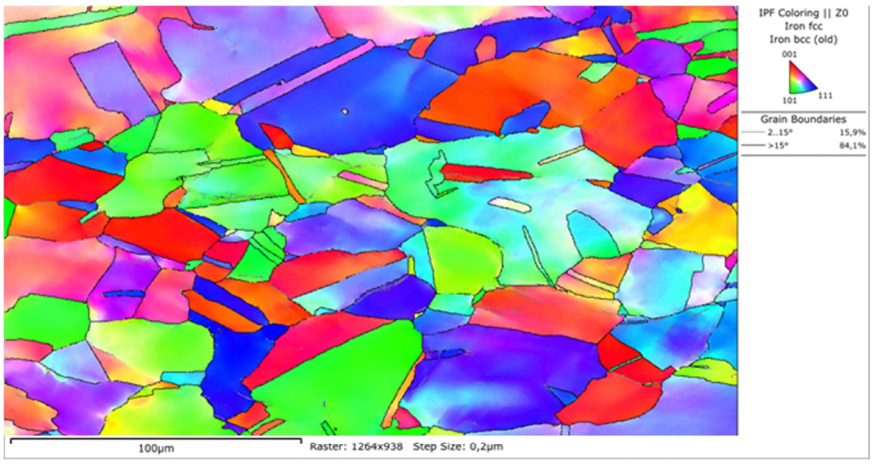

HAZ IPF map (Point 1)

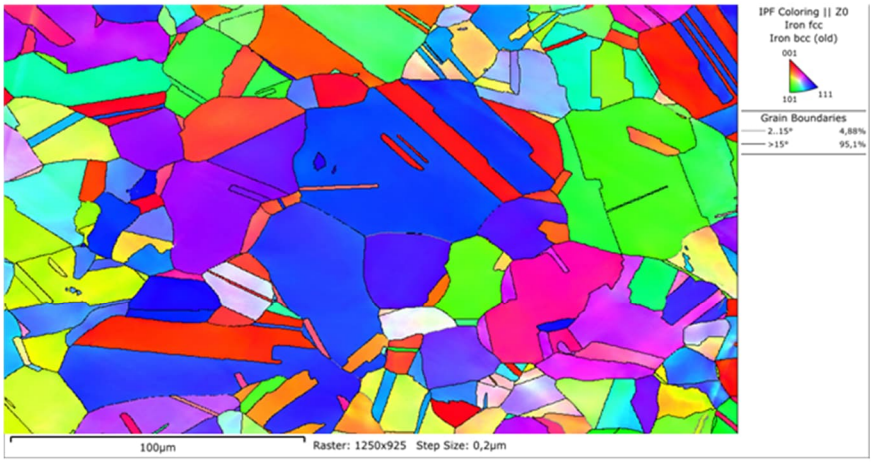

HAZ IPF map (Point 2)

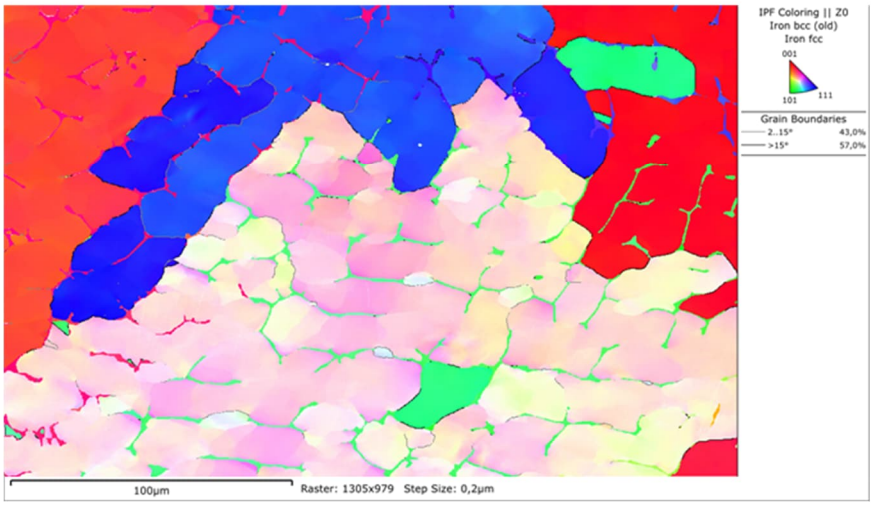

Fusion Zone IPF map (Point 3)

Figure 9. IPF maps showing grain structures in HAZ points 1 and 2, and fusion zone in as-welded sample.

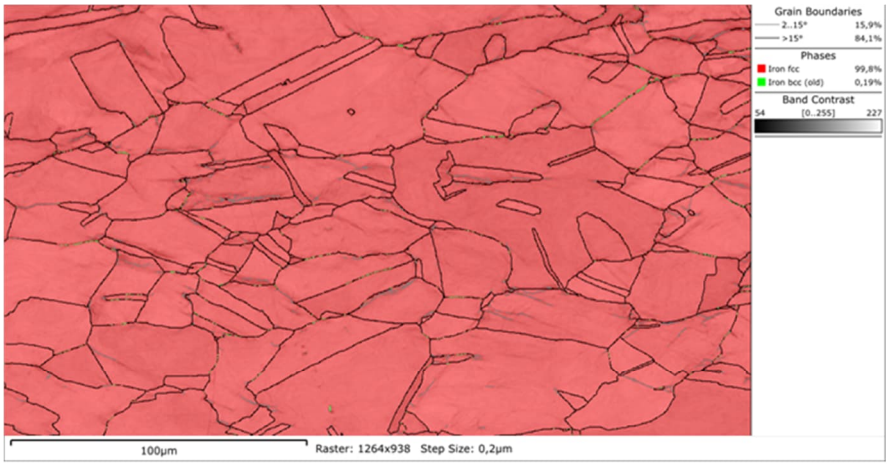

HAZ Phase map (Point 1)

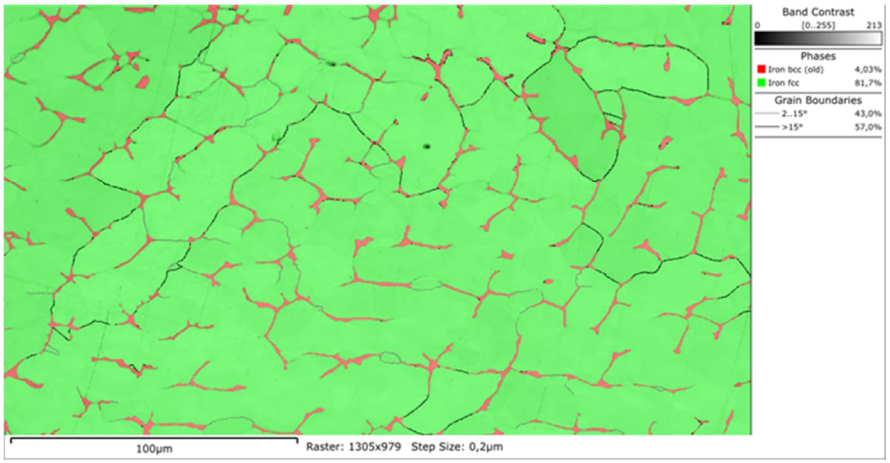

Fusion Zone Phase map (Point 3)

Figure 10. Phase maps showing delta ferrite in the HAZ point 1 (< 1 %) and fusion zone (4 %) in as-welded sample.

3.2.2 Thermally cycled (500 °C) sample after autoclave exposure test

Misorientation (MO) average maps

Thermal cycling was performed to introduce tensile residual stresses to weld samples before autoclave exposure tests. However, no cracking was observed in the samples after the autoclave tests although, the highest tensile residual stresses measured before the autoclave tests were about 500 MPa. After the autoclave exposure test, there were high amount of misorientation left in HAZ (point 2) and in weld (point 3) indicating that the stresses were not relaxed during the autoclave exposure test (Figure 11). This is in accordance with the residual stress measurements.

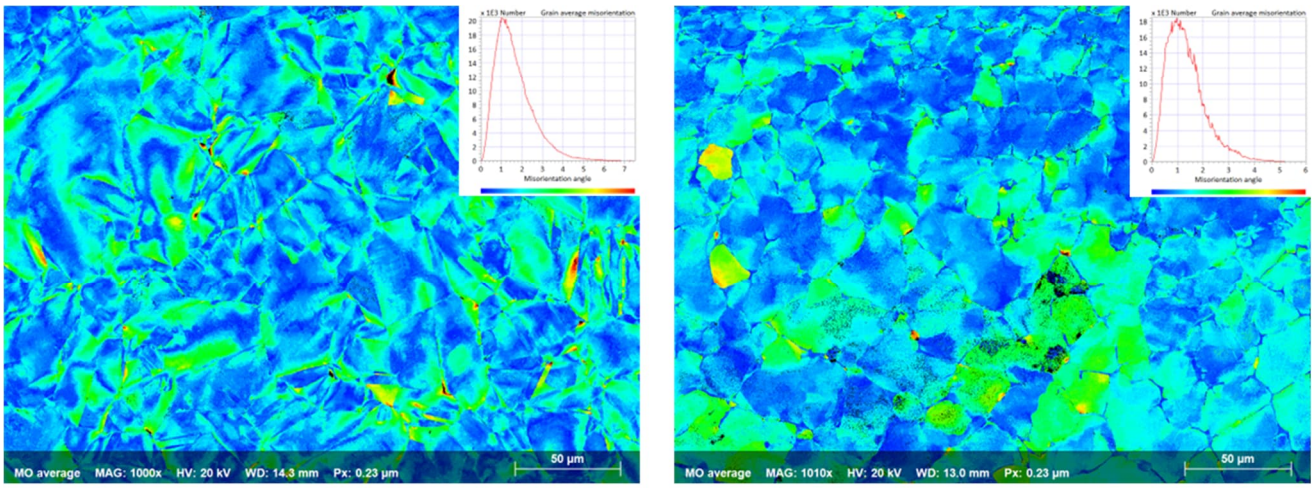

HAZ MO average map (Point 2) Fusion Zone MO average map (Point 3)

Figure 11. MO average maps of 500 °C thermally cycled weld sample after autoclave exposure test measured from HAZ and fusion zone.

3.3 Microhardness measurements

Vickers microhardness measurements were performed on the as-welded sample and for the autoclave tested (AC) sample thermally cycled at 500° C to evaluate localized mechanical properties across different microstructural regions.

3.3.1 As-welded condition

Three test lines were measured with 60 indentation points each with HV0.02 scale from the as-welded sample. The purpose was to measure hardness variation within the grains across the HAZ due to thermal cycles during the welding process. The positions of test lines are presented in Figure 12.

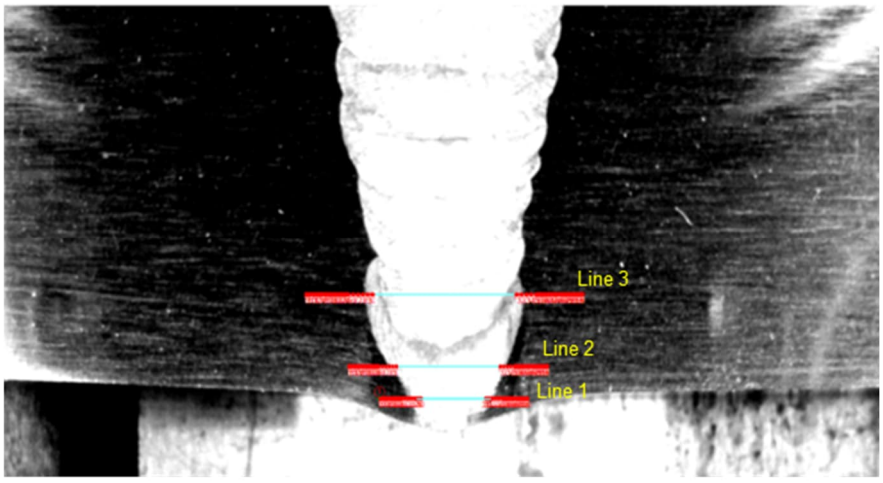

Figure 12. Test line 1, 2, and 3 positions for HV0.02 hardness measurements.

Microhardness profile: test line 1

Figure 13 shows an optical micrograph showing the FGHAZ, CGHAZ, and weld fusion zone on the left side of test line 1.

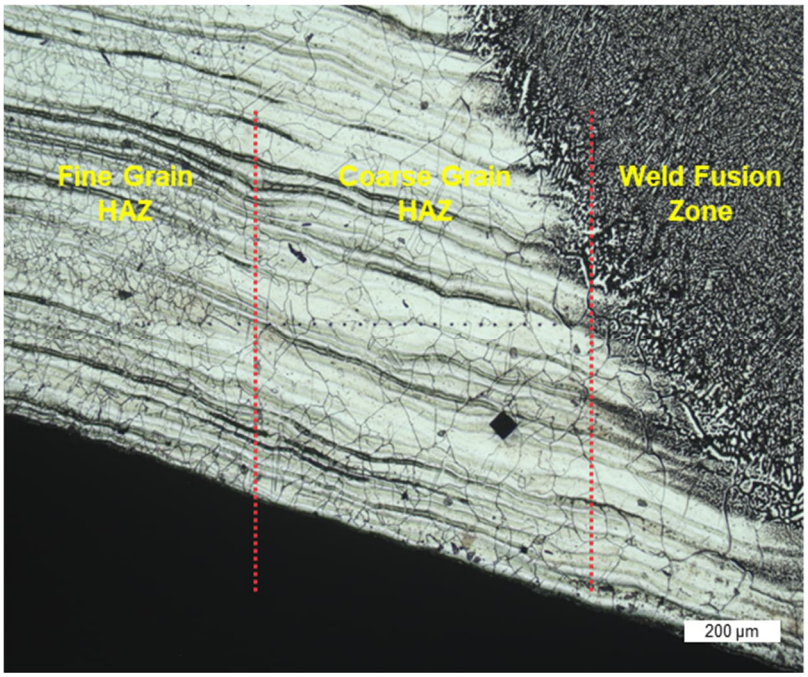

Figure 13. Microstructure and HAZ regions of the as-welded sample showing fine grain HAZ, coarse grain HAZ, and weld fusion zone of left side of test line 1.

Figure 14 presents the hardness profile measured along test line 1.

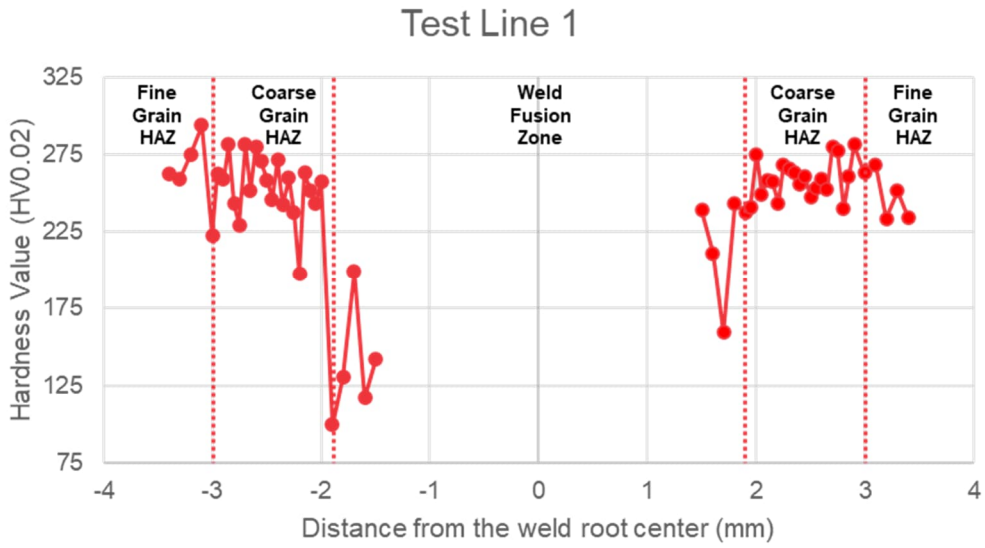

Figure 14. Microhardness profile (HV0.02) measured along test line 1 from as-welded sample.

Table 8 presents the average hardness values in different regions along test line 1. The fusion zone exhibited the lowest hardness (178 HV0.02), while the FGHAZ and CGHAZ on either side of the weld exhibited higher values (250 HV0.02), suggesting strain hardening due to welding process (welding deformation). Individual soft points, having hardness about 100 HV0.02 or lower, were found in weld close to the fusion line, but they are considered as a results of etching of the fusion zone.

Table 8. Average HV0.02 values across test line 1.

Zone	Average hardness (HV0.02)
FG HAZ (left) – 5 points	263
CG HAZ (left) – 20 points	255
Weld fusion zone – 5+5 points	178
CG HAZ (right) – 20 points	260
FG HAZ (right) – 5 points	250

Figure 15 presents the individual hardness values within the FGHAZ and CGHAZ on the left side of test line 1, showing the grain size variation across the HAZ.

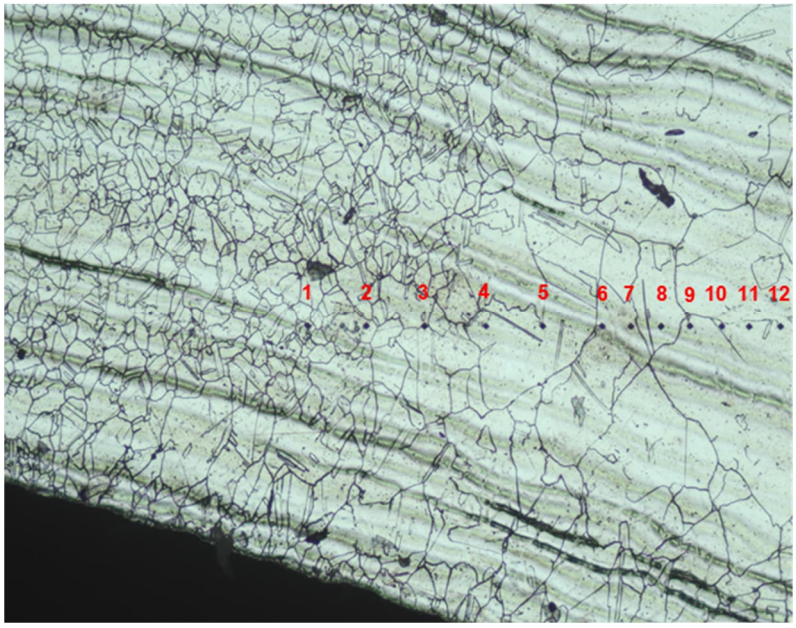

Measurement point	Line 1 (HV0.02)
1	262
2	259
3	274
4	294
5	222
6	262
7	259
8	281
9	243
10	229
11	281
12	252

Figure 15. Grain size variation in HAZ and individual hardness values on the left side of test line 1.

Microhardness profile: test line 2

Figure 16 presents the hardness profile along test line 2.

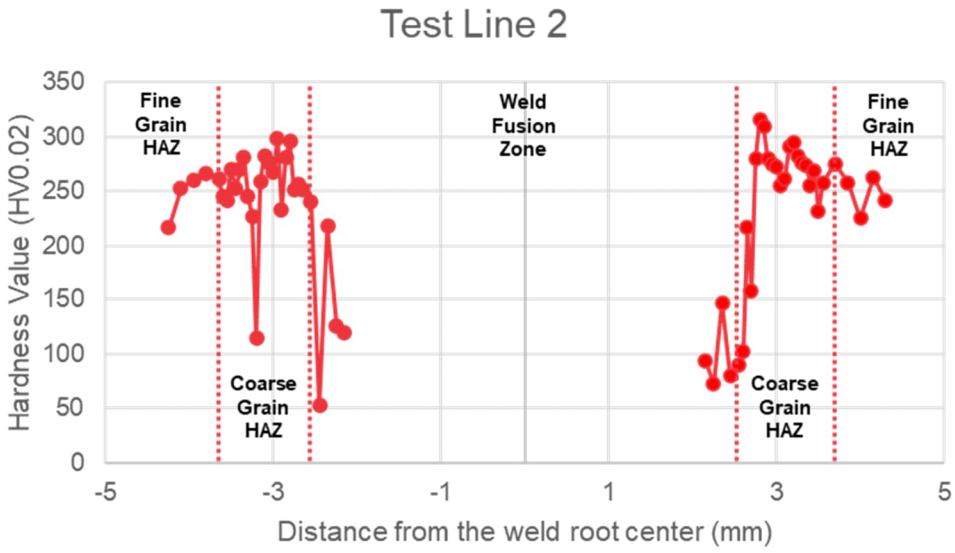

Figure 16. Microhardness profile (HV0.02) measured along test line 2 from as-welded sample.

Table 9 shows the average HV0.02 values across the different zones measured along test line 2. The HAZ region exhibited again higher hardness than the weld zone. Individual soft point were also found in the test line 2. Hardness values measured within the FGHAZ and CGHAZ on the left side of test line 2 are presented in Figure 17.

Table 9. Average HV0.02 values across test line 2.

Zone	Average hardness (HV0.02)
FG HAZ (left) – 5 points	252
CG HAZ (left) – 20 points	255
Weld fusion zone – 5+5 points	124
CG HAZ (right) – 20 points	258
FG HAZ (right) – 5 points	252

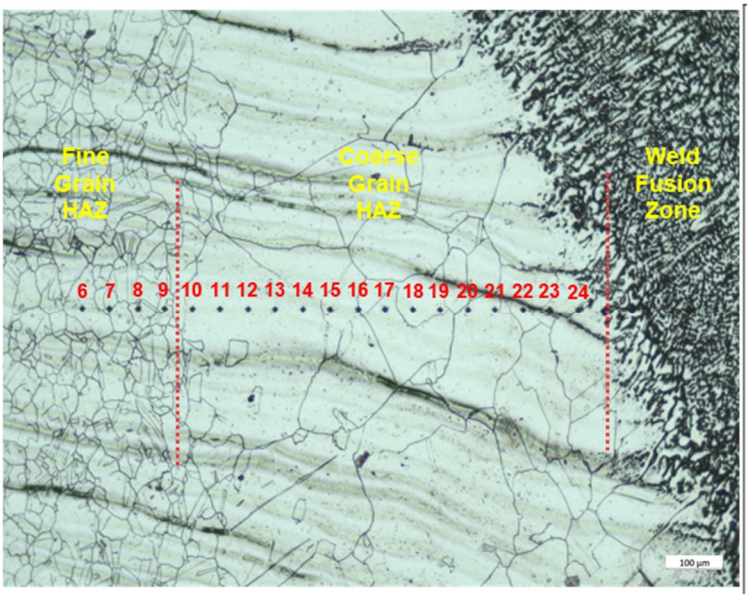

Measurement point	Line 2 (HV0.02)
6	244
7	241
8	269
9	25
10	269
11	280
12	245
13	226
14	114
15	258
16	282
17	275
18	267
19	298
20	233
21	281
22	295
23	251
24	256

Figure 17. Grain size variation in HAZ and individual hardness values on the left side of test line 2.

Microhardness profile: test line 3

Figure 18 presents the hardness profile along test line 3.

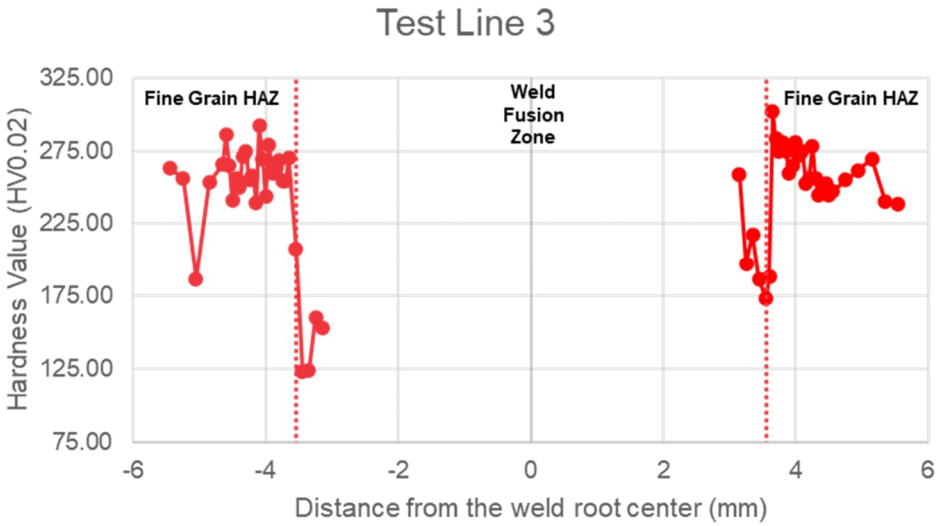

Figure 18. Microhardness profile (HV0.02) measured along test line 3 from as-welded sample.

Table 10 shows the average hardness values for the different regions along test line 3. The weld fusion zone again exhibits the lowest hardness (180 HV0.02), while the HAZ exhibited higher values, being typically higher than 250 HV0.02.

Table 10. Average HV0.02 values across test line 3.

Zone	Average hardness (HV0.02)
FG HAZ (left) – 5 points	245
CG HAZ (left) – 20 points	262
Weld fusion zone – 5+5 points	180
CG HAZ (right) – 20 points	262
FG HAZ (right) – 5 points	253

Figure 19 presents the hardness values within the grains on the right side of the test line 3. The HAZ hardness values were about the same along all test lines 1, 2, and 3. No dependence of hardness values in the location of measurements close to grain boundaries or inside the grains was found in either of the test lines 1-3. The full table of hardness values in test lines is presented in appendix.

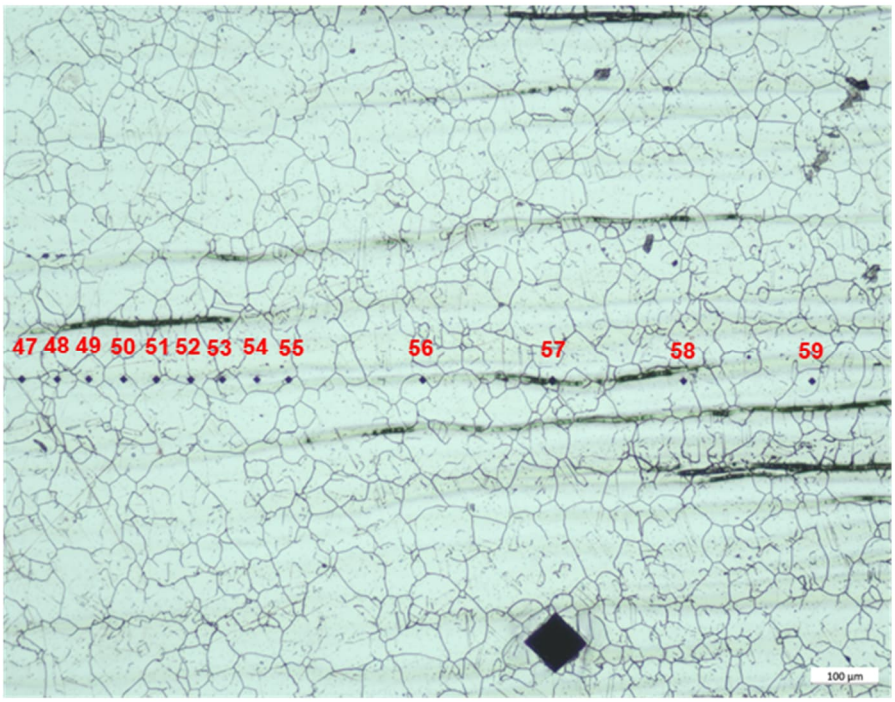

Measurement point	Line 3 (HV0.02)
47	252
48	256
49	278
50	256
51	245
52	251
53	253
54	245
55	247
56	255
57	261
58	269
59	240

Figure 19. HAZ microstructure and individual hardness values on the right side of test line 3.

3.3.2 Thermally cycled sample (500 °C) after autoclave test

Positions of HV1 hardness profiles measured from the autoclave exposure tested 500° C thermally cycled sample are presented in Figure 20 together with the hardness profiles measured from the as-welded sample. The measured hardness profiles are presented in Figure 21. In the as-welded sample, the hardness values were the greatest in the weld root location being of order of 250 HV1 at maximum. The lowest hardness values in the weld were measured on the bead side, being below 200 HV1. The hardness of the base material was about 180 HV1, which is typical for a 316L pipe material in solution annealed condition. When approaching to HAZ, the hardness increased to a level of about 250 HV1, which is the same order as in HV0.02 measurements. When measured after the autoclave exposure test, the hardness values of the 500 °C thermally cycled sample were in the same range than in the as-welded condition.

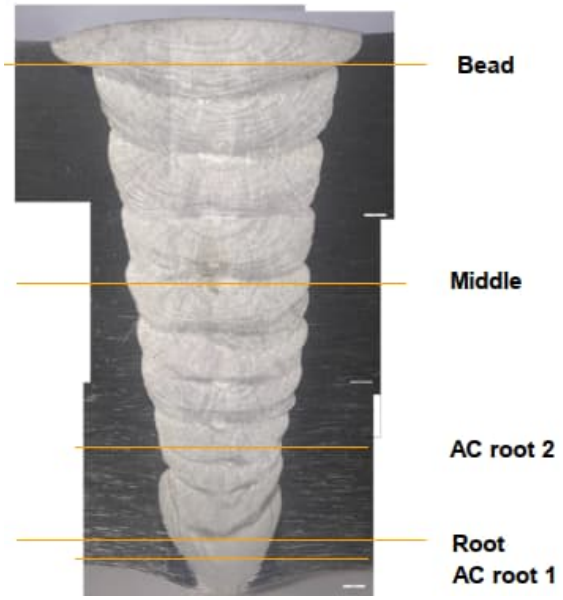

Figure 20. Vickers HV1 line patterns measured from as-welded sample and from 2 locations in 500 °C autoclave tested sample (AC).

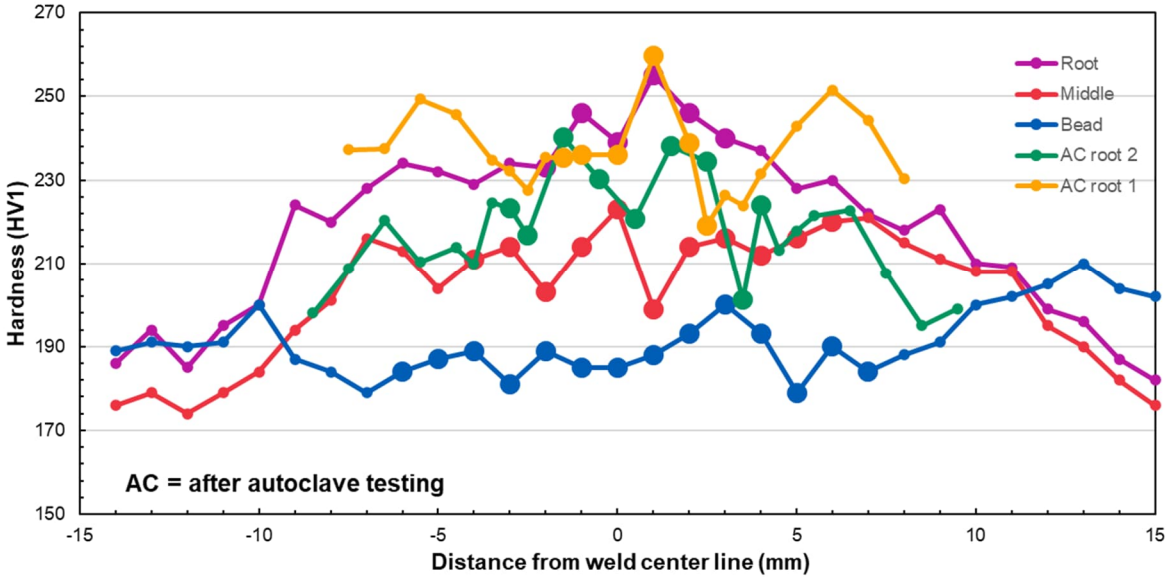

Figure 21. Vickers HV1 results for as-welded and autoclave tested samples (AC). Measurement location in samples: small marker = base metal, big marker = weld.

4 Conclusions

This study investigated properties and microstructure of the 316L steel pipe weld, which was manufactured so that it represented that of OL3 primary circuit. The samples studied were the was-welded condition and autoclave exposure tested samples, which were thermally cycled before the autoclave exposure tests. The investigation consisted of XRD residual stress measurements, SEM EBSD, LOM, and Vickers microhardness measurements. The results are summarized below.

Residual stress measurements of the as-welded sample showed compressive residual stresses at the weld centreline. When approaching to the fusion line, they changed to tensile

stresses and remained as tensile stresses in HAZ. After that, they changed to compressive again. After thermal cycling and subsequent autoclave exposure tests, the shape of the residual stress patterns were similar to that of the as-welded condition. The 500 °C thermally cycled sample exhibited the highest tensile stresses, being about 500 MPa. After autoclave exposure test at 325 °C for 4 weeks, the samples did not show tensile relaxation. Principal stresses and their direction were calculated from the results.

The SEM and LOM investigations revealed clear microstructural variations across the CGHAZ, FGHAZ, and fusion zone, highlighting the influence of welding thermal cycles on grain morphology, misorientation, and phase distribution. In the as-welded condition, the CGHAZ exhibited high misorientation and elongated grains, reflecting residual stresses from thermal exposure due to welding deformation, while the grains within FGHAZ were equiaxed due to recrystallization. The fusion zone exhibited a typical welded austenitic steel microstructure with 4-8 % delta ferrite, which is considered to increase resistance to SCC. Base material delta ferrite content was below 1 %. After autoclave exposure test, both HAZ and fusion zone displayed increased average misorientation in the 500 °C thermally cycled sample, suggesting that the residual stresses were not relaxed during the exposure test.

Microhardness measurements across the weld local variation in hardness across the fusion zone, CGHAZ, and FGHAZ. In the HAZ, the average hardness was typically about 250 HV0.02. No significant difference was observed between CGHAZ and FGHAZ. In HV0.02 measurements, soft regions were found within the fusion zone close to the fusion line where the average hardness varied between 124 -180 HV0.02. The etching of the fusion zone has probably affected to the lowest HV0.02 values. The location of the measurement point, whether at the grain boundaries or inside the grain, did not have a noticeable effect on the hardness values. However, hardness variation between the HAZ and the fusion zone can increase risk for SCC. Soft points within the fusion zone were not observed in HV1 measurements, but otherwise the HV1 and HV0.02 results were within the same range.

References

[1] J. H. Shin, “Effect of Thermo-Mechanical Processing on Initiation and Propagation of Stress Corrosion Cracking in 304L Austenitic Stainless Steel”, *Metals 2023, Vol. 13, Page 1458*, vol. 13, no. 8, p. 1458, Aug. 2023, doi: 10.3390/MET13081458.

[2] S. A. Abubakar, S. Mori, and J. Sumner, “A Review of Factors Affecting SCC Initiation and Propagation in Pipeline Carbon Steels”, *Metals 2022, Vol. 12, Page 1397*, vol. 12, no. 8, p. 1397, Aug. 2022, doi: 10.3390/MET12081397.

[3] T. Saukkonen, M. Aalto, I. Virkkunen, U. Ehrnstén, and H. Hänninen, “Plastic strain and residual stress distributions in an AISI 304 stainless steel BWR pipe weld”, *15th International Conference on Environmental Degradation of Materials in Nuclear Power Systems-Water Reactors 2011*, vol. 3, pp. 2221–2237, 2011, doi: 10.1007/978-3-319-48760-1_142.

[4] A. Mazhar, “Residual Stress and Stress Corrosion Cracking of Austenitic Stainless Steels in Nuclear Environments”, M.Sc. Thesis, Aalto University, 2024.

[5] A. Mazhar, R. Ilola, I. Virkkunen, “SCC tests for thermally cycled specimens and metallographic characterization”, Safer 2028 Research Report, 2024.

Appendix. Results of HV0.02 microhardness measurements

Table A1. Hardness values in HAZ region of as-welded sample (test line 1).

Measurement point	Distance from the weld root center (mm)	Line 1 (HV0.02)
1	-3.4	263
2	-3.3	259
3	-3.2	275
4	-3.1	294
5	-3	223
6	-2.95	263
7	-2.9	259
8	-2.85	282
9	-2.8	244
10	-2.75	230
11	-2.7	282
12	-2.65	252
13	-2.6	280
14	-2.55	271
15	-2.5	259
16	-2.45	246
17	-2.4	272
18	-2.35	242
19	-2.3	260
20	-2.25	237
21	-2.2	198
22	-2.15	263
23	-2.1	252
24	-2.05	243
25	-2	258
26	-1.9	100
27	-1.8	130
28	-1.7	199
29	-1.6	117
30	-1.5	142
31	1.5	239
32	1.6	211
33	1.7	159
34	1.8	243
35	1.9	238
36	1.95	241
37	2	276
38	2.05	250
39	2.1	259
40	2.15	258
41	2.2	244
42	2.25	269
43	2.3	266
44	2.35	263
45	2.4	256
46	2.45	261
47	2.5	247
48	2.55	253
49	2.6	259
50	2.65	253
51	2.7	280
52	2.75	278
53	2.8	240
54	2.85	261
55	2.9	282
56	3	263
57	3.1	268
58	3.2	234
59	3.3	251
60	3.4	235

Table A2. Hardness values in HAZ region of as-welded sample (test line 2).

Measurement point	Distance from the weld root center (mm)	Line 2 (HV0.02)
1	-4.25	217
2	-4.1	252
3	-3.95	261
4	-3.8	266
5	-3.65	262
6	-3.6	245
7	-3.55	241
8	-3.5	269
9	-3.45	253
10	-3.4	270
11	-3.35	281
12	-3.3	246
13	-3.25	226
14	-3.2	115
15	-3.15	259
16	-3.1	282
17	-3.05	276
18	-3	267
19	-2.95	298
20	-2.9	233
21	-2.85	281
22	-2.8	296
23	-2.75	252
24	-2.7	256
25	-2.65	252
26	-2.55	240
27	-2.45	53
28	-2.35	218
29	-2.25	126
30	-2.15	119
31	2.15	93
32	2.25	72
33	2.35	147
34	2.45	80
35	2.55	90
36	2.6	102
37	2.65	217
38	2.7	158
39	2.75	279
40	2.8	315
41	2.85	309
42	2.9	280
43	2.95	275
44	3	273
45	3.05	255
46	3.1	261
47	3.15	290
48	3.2	294
49	3.25	283
50	3.3	276
51	3.35	273
52	3.4	255
53	3.45	269
54	3.5	231
55	3.55	257
56	3.7	275
57	3.85	258
58	4	225
59	4.15	263
60	4.3	241

Table A3. Hardness values in HAZ region of as-welded sample (test line 3).

Measurement point	Distance from the weld root center (mm)	Line 3 (HV0.02)
1	-5.45	263
2	-5.25	256
3	-5.05	187
4	-4.85	253
5	-4.65	266
6	-4.6	286
7	-4.55	265
8	-4.5	241
9	-4.45	256
10	-4.4	250
11	-4.35	271
12	-4.3	275
13	-4.25	255
14	-4.2	258
15	-4.15	240
16	-4.1	292
17	-4.05	269
18	-4	243
19	-3.95	279
20	-3.9	259
21	-3.85	263
22	-3.8	268
23	-3.75	254
24	-3.7	254
25	-3.65	270
26	-3.55	208
27	-3.45	123
28	-3.35	124
29	-3.25	160
30	-3.15	153
31	3.15	258
32	3.25	197
33	3.35	217
34	3.45	186
35	3.55	173
36	3.6	188
37	3.65	302
38	3.7	283
39	3.75	274
40	3.8	281
41	3.85	274
42	3.9	260
43	3.95	265
44	4	281
45	4.05	272
46	4.1	274
47	4.15	252
48	4.2	256
49	4.25	278
50	4.3	256
51	4.35	245
52	4.4	251
53	4.45	253
54	4.5	245
55	4.55	247
56	4.75	255
57	4.95	261
58	5.15	269
59	5.35	240
60	5.55	238